CHEMISTRY OF MATERIALS

Article

pubs.acs.org/cm

New Strategy for the Growth of Complex Heterostructures Based on Different 2D Materials

Mattia Cattelan,[†] Brian Markman,[‡] Giacomo Lucchini,[†] Pranab Kumar Das,[§,∥] Ivana Vobornik,[§] Joshua Alexander Robinson,[‡] Stefano Agnoli,*[,†] and Gaetano Granozzi[†]

[†]Department of Chemical Sciences, University of Padova, via Marzolo 1, Padova 35131, Italy

[‡]Department of Materials Science and Engineering and Center for 2-Dimensional and Layered Materials, The Pennsylvania State University, University Park, Pennsylvania 16802, United States

[§]CNR-IOM, TASC Laboratory, AREA Science Park Basovizza, 34149 Trieste, Italy

[∥]International Centre for Theoretical Physics, Strada Costiera 11, 34100 Trieste, Italy

ABSTRACT: Tungsten disulfide (WS_2) monolayers have been synthesized under ultra high vacuum (UHV) conditions on quasi-free-standing hexagonal boron nitride (h-BN) and gold deposited on Ni(111). We find that the synthesis temperature control can be used to tune the WS_2 structure. As documented by in situ core level and valence band photoemission and by ex situ Raman spectroscopy, the partially disordered WS_2 layer obtained at room temperature transforms to the 2H-WS_2 phase at about 400 °C. Low energy electron diffraction confirms the existence of van der Waals epitaxy between WS_2 and h-BN and gold substrates. The measured band structure indicates that the WS_2 electronic structure is not affected by the interaction with the h-BN and gold substrates.

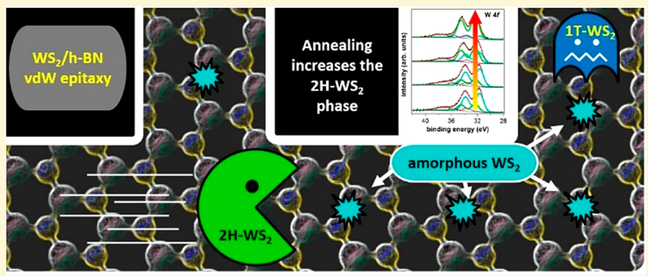

■ INTRODUCTION

Since the isolation of monolayer graphene by Geim and Novosëlov in 2004,[1] two-dimensional materials have received major attention. In particular, interest in hexagonal boron nitride (h-BN) and transition metal dichalcogenides (TMDs) has surged in recent years due to their wide range of electronic properties ranging from insulating (h-BN) to semiconducting (TMDs). Moreover, monolayer systems of h-BN and TMDs offer interesting optical and electronic properties that differ from their bulk counterparts.[2−5] Monolayer semiconducting TMDs are attractive candidates for future optoelectronics, including flexible electronics,[2,6,7] and even spintronics.[8] Additionally, MoS_2 and WS_2 are already widely used in catalytic applications including hydrotreating, hydrocracking,[9] and hydrogen evolution reaction (HER).[10,11] However, h-BN exhibits a bandgap of 5.97 eV,[12] making it an attractive candidate for solar blind detectors, UV lasers, low-k dielectric materials for 2D devices,[13−16] and when coupled with magnetic metal substrates can exhibit ferrimagnetism.[17]

Currently, the focus is on heterogeneous systems, called van der Waals heterostructures, where monolayers of different 2D materials are stacked vertically layer-by-layer, or stitched together seamlessly in-plane to form lateral heterojunctions. Many physical properties have been explored in such van der Waals heterostructures, and devices with improved performances have been demonstrated.[5,18−22] For example, monolayer TMD heterostructures artificially stacked by mechanical transfer techniques,[5] i.e., WS_2/MoS_2[23,24] and WSe_2/MoS_2,[25] exhibit interlayer coupling that enables electron−hole recombination between layers that modifies their optoelectronic properties. By placing h-BN layers in between TMD layers, the coupling can be modulated.[25] However, fabrication of 2D heterostructures with clean and sharp interfaces, essential for preserving their intrinsic properties, remains a challenge.

Mechanical transfer methods have major drawbacks: the stacking orientation cannot be precisely controlled, the interface between layers can be easily contaminated,[26] and the presence of metal or polymer residues in contact with the 2D layers modifies their pristine properties[27,28] and the characteristics of the desired heterojunctions.[6] However, there are still only a few reports of directly grown 2D heterostructures with TMDs,[29−31] indicating that a concerted effort is needed in developing direct growth methods of these structures.[32] Single layer WS_2 has been obtained by chemical vapor deposition (CVD) on transferred h-BN,[33] whereas WS_2/MoS_2 in-plane and stacked heterojunctions have been grown by CVD.[34] The production method of 2D heterostructures is a crucial factor for their future scale-up and implementation into industrial applications. As a result, CVD and molecular beam epitaxy (MBE)[35] techniques may be considered industrial standards for building advanced device structures.

Received: March 30, 2015
Revised: May 12, 2015
Published: May 12, 2015

DOI: 10.1021/acs.chemmater.5b01170
Chem. Mater. 2015, 27, 4105−4113

MoS_2 has been widely investigated,[36] however other TMDs such as WS_2 have received less attention. Two of the most characteristic phases of WS_2 are the 1T (octahedral) and 2H (trigonal prismatic) phases.[37] The former is metallic and metastable, whereas the latter is semiconducting and thermodynamically favored. Because of its instability, the 1T phase can be irreversibly converted into the 2H polymorph by annealing at 300−400 °C.[10] The 1T phase can be formed from bulk 2H crystals by intercalating alkali metals,[10] or by irradiation with high-energy electrons, as in transmission electron microscopy (TEM).[37] The 1T-WS_2 metallic phase is important because its conductive behavior boosts the activity for HER, achieving performance comparable to commercial platinum catalysts.[10] Thus, recent research has focused on direct deposition and stabilization of the metastable metallic phase. Because of the disadvantages of the alkali metal intercalation (partial damage of the layer by strain[30] and reactions to form Li_2S[38]), some recently proposed methods include colloidal synthesis[39] and stabilization via donor doping.[40]

In this paper, we report the synthesis of single layer WS_2 on quasi-free-standing h-BN (i.e., h-BN/Au/Ni(111)) and on a traditional "3D" substrate Au/Ni(111) and demonstrate the realization of new artificially stacked solids. The syntheses were carried out in ultra high vacuum (UHV) in order to study the pristine properties and to create stacked heterojunctions without air contamination/oxidation or the presence of residue as result of transfer procedures.[26] We find that the structure of the WS_2 is "tunable", as it depends strongly on the synthesis temperature. For WS_2 films grown at low temperatures, we find that the XPS data are consistent with the presence of 1T-WS_2, which subsequently transforms into 2H-WS_2 at temperatures comparable to those reported for 1T → 2H phase transition;[10] however, Raman spectroscopy, low energy electron diffraction (LEED) and valence band (VB) ultraviolet photoemission spectroscopy (UPS) data indicate the presence of a disordered structure formed by both amorphous and 2H-WS_2 phases at low temperatures. Our data suggest that the XPS signal attributed to the 1T phase in previous reports,[10,39,41] may be partly due to the presence of amorphous WS_2.

Our data are comparable to a previous scanning tunneling microscopy (STM) study where the growth of few-nanometer wide single layer WS_2 islands on Au(111) was observed:[42] the deposition of WS_2 at low temperature leads to a disordered structure, while thermal treatment triggers the formation of ordered 2H-WS_2. Another work[43] presented a valence band study of bulk and single layer 2H-WS_2 supported on highly oriented pyrolytic graphite (HOPG). This demonstrates that highly controlled single layer films of WS_2 can be grown under UHV conditions on several substrates by carefully controlling the growth procedure; however, a complete photoemission study, from core level to valence band, of the evolution from disordered to ordered WS_2 on a "3D" and "2D" substrates is missing in the literature.

■ EXPERIMENTAL SECTION

Samples were prepared and examined in situ in UHV ($<10^{-9}$ mbar) by XPS, to determine the surface composition, UPS, to study the VB structure, LEED, to determine the degree of the long-range order, and ex situ by Raman spectroscopy, to confirm the presence of 2H-WS_2. Typically, the tungsten 4*f* (W 4*f*) photoemission line is exploited to understand which polymorph of WS_2 has been obtained, and its evolution with the annealing temperature is used to characterize the structural changes.[10,39,41] Additionally, TEM,[10] X-ray diffraction (XRD),[39] or Raman spectroscopy are used to confirm the octahedral environment for W, but these techniques cannot exclude a priori the presence of a disordered part in the layer.

Materials Preparation. To synthesize the 2D heterostructures, a Ni(111) single crystal substrate was chosen because it allows facile growth of high quality h-BN layers in UHV; the resulting layer can also be electronically decoupled by intercalating gold underneath.[44] The Ni(111) single crystal was cleaned by repeated cycles of sputtering (1.5 kV, 1×10^{-6} mbar of Ar) and annealing at 800 °C; the surface cleanliness was verified by photoemission and LEED. h-BN monolayers were synthesized by dosing 2×10^{-7} mbar a borane−ammonia complex (NH_3−BH_3) on the Ni(111) at 700 °C. The precursor was placed in a flanged glass tube, heated at 80 °C, and dosed via a leak valve. In order to intercalate gold underneath h-BN, few layers of Au (about 6 ML) were deposited on h-BN/Ni(111) surface, while annealing the crystal at 400 °C, using electron-beam evaporation.

Tungsten disulfide layers were obtained by evaporating W in an atmosphere of 2×10^{-8} mbar of sulfur vapor, while annealing the sample at 120 °C and post treating at 400 °C to achieve the semiconducting trigonal prismatic phase (2H).[40] It is also possible to obtain directly 2H-WS_2 by depositing W in the presence of S vapor while annealing the crystal at 400 °C. Sulfur vapors were obtained by placing elemental sulfur in a glass vial connected to the main preparation chamber via a gate valve. The introduced sulfur is likely of the form S_6 or S_8 clusters.[45] The use of sulfur, instead of H_2S[42] has been chosen for safety of the operator, H_2S is a highly toxic and flammable gas, and because of the low pressure necessary to fully sulfurize W layers deposited at rate of about 0.1 ML/min. This is probably due to the higher oxidation number of the sulfur chains with respect to the already reduced H_2S; the sulfurization reaction of metallic W is facilitated by this redox reaction.

Both tungsten and gold evaporation rates were calibrated using angle resolved XPS measurements according to the method reported in ref 46. A crosscheck of the amount of deposited material has also been carried out by XPS after film preparation.

Characterization. All XPS lines were acquired with a conventional Al K_α source with pass energy (PE) of 20 eV; the BE scale was calibrated by normalizing the Au $4f_{7/2}$ binding energy (BE) position to 84.0 eV. Photoemission lines were separated into single chemically shifted components (after Shirley background subtraction) using symmetrical Voigt functions with a full width at half-maximum (fwhm) of 1.35 eV. VB spectra were acquired with a standard Helium discharge source with PE = 2 eV for He I and PE = 10 eV for He II, spectra were acquired in the Γ direction of the Brillouin zone (i.e., normal emission) with an analyzer angular acceptance of 3°. Angle resolved photoemission spectroscopy (ARPES) measurements were accomplished at the ELETTRA beamline APE with photons of 40 eV, PE = 10 eV and energy resolution of 20 meV, the electron analyzer angular resolution was better than 0.2°. Raman spectra were acquired with a ThermoFisher DXR Raman microscope using a 532 nm laser (1 mW), focused on the sample with a 50× objective (Olympus) obtaining a spot size of about 1 μm.

■ RESULTS AND DISCUSSION

We have investigated, in a systematic way, the different types of interfaces that arise from growing WS_2 on "2D" and "3D" substrates, with the aim of understanding the effects originating from variations in electronic coupling. Following a strict reductionist approach, we have studied in detail the following heterostructures h-BN/Ni(111), h-BN/Au/Ni(111), WS_2/Au/Ni(111), and finally WS_2/h-BN/Au/Ni(111). In this context, h-BN and gold represent the prototypical atomic thin insulating layer and "3D" metal contact, respectively. In the following pages, the results of each different interface will be reported separately.

DOI: 10.1021/acs.chemmater.5b01170
Chem. Mater. 2015, 27, 4105−4113

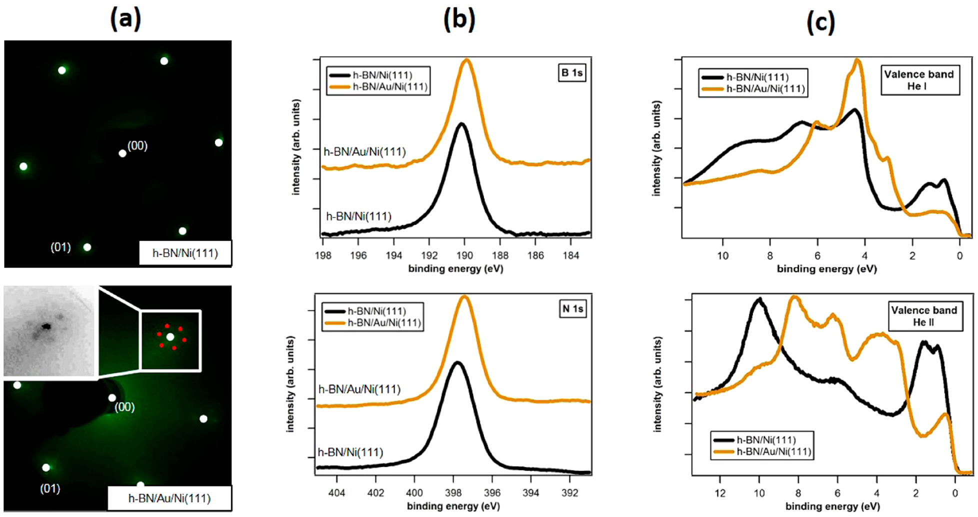

Figure 1. (a) LEED images, acquired at 70 eV, of h-BN/Ni(111) (1 × 1) reconstruction, h-BN/Au/Ni(111) a (9 × 9), the inset shows a magnified view of 6-fold h-BN diffraction spots around one of the substrate integer diffraction beams. (b) Photoemission from B 1*s* and N 1*s* core levels and (c) VB photoemission spectra acquired with He I and He II source of h-BN/Ni(111) and h-BN/Au/Ni(111).

Growth of h-BN/Ni(111) and h-BN/Au/Ni(111). As explained in the Experimental Section, h-BN layers on clean Ni(111) were obtained by dehydrogenation of the borane-ammonia complex. Recently, it has been demonstrated that this molecule can be fully dehydrogenated to h-BN at high temperature.[47] Our data are comparable to the literature,[44,48] where the borazine precursor was used.

The h-BN deposition is self-limiting to 1 ML and is characterized by a (1 × 1) structure with respect to the Ni(111) surface (as visible in Figure 1a); a deposition time of 10 min was used to ensure complete coverage. The insulating h-BN is tightly chemically bound to Ni substrate,[17] but can be decoupled by intercalating gold in order to reach a quasi-freestanding state.[44] In order to do so, few layers (about 6 ML) of Au were deposited on the h-BN/Ni(111) surface, while annealing the crystal at 400 °C. The LEED patterns of h-BN/Ni(111) and h-BN/Au/Ni(111) are reported in Figure1a. In the sample intercalated by Au, multiple diffraction spots with 6-fold symmetry can be observed around the integer reflections indicating the formation of an ordered (9 × 9) moiré superstructure between the unstrained h-BN and the Au(111) surface. The effect of gold intercalation can also be seen in the N 1*s* and B 1*s* photoemission lines (Figure 1b), that are shifted to lower BEs, and also in VB spectra (Figure 1c), where the h-BN π band moves from 9.9 to 8.2 eV, whereas the σ band shifts from 5.8 eV to about 4 eV, in agreement with ref 44. These electronic changes are related to the elimination of the chemisorption bonds between h-BN and Ni atoms and to the strain associated with the (1 × 1) epitaxy on Ni(111), in favor of relaxed physisorption of h-BN on the Au layer.

Growth of WS_2/Au/Ni(111). Monolayer WS_2 was grown on Au/Ni(111) at 120 °C and then annealed at 200 °C, 300 °C, and 400 °C; the effects of the thermal treatment on the W 4*f* photoemission lines is reported in Figure 2. The elemental composition of the deposited layer was determined by considering the integrated intensity of S 2*p* and W 4*f* photoemission peaks and using as an internal reference, an ex situ bulk sample of stoichiometric WS_2. It was found that the WS_2/Au/Ni(111) system composition, when deposited at 120 °C, was $WS_{2.9}$. The annealing process decreased the S/W ratio to $WS_{2.5}$. The WS_{2+x} stoichiometry can be explained by the presence of nanometer domains, whose edges are S terminated, and by S adsorption on the substrate surface.[42] As the sample is annealed, the area of the WS_2 islands increases, while reducing the area of edges.[11,42] Moreover, the annealing process desorbs adventitious S that was deposited due to residual sulfur background.

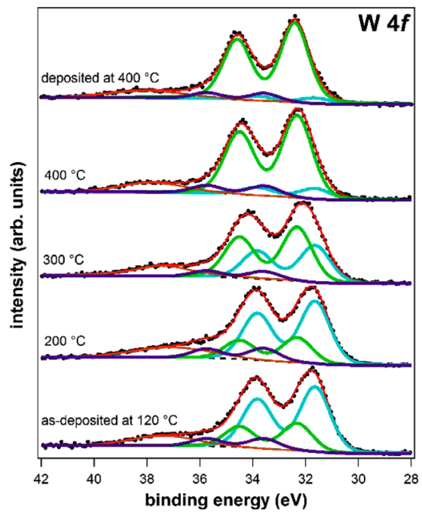

Figure 2. W 4*f* photoemission spectra of WS_2/Au/Ni(111): as-deposited at 120 °C and subsequently annealed at 200, 300, and 400 °C, or directly deposited at 400 °C. Measured data, Shirley background and total fit are represented with black dots, dashed black line and solid red line, respectively. Photoemission lines for amorphous WS_2, 2H-WS_2, WS_3, and W $5p_{3/2}$ are shown with blue, green, purple, and brown solid lines, respectively.

No LEED pattern was discernible when depositing WS_2 at 120 °C while, after post treatment at 400 °C faint hexagonal diffraction spots were visible. To obtain a better diffraction pattern, WS_2 can be deposited directly on Au/Ni(111) at 400 °C. In this way, the W atoms have higher mobility and therefore can attain a more ordered and energetically stable structure. The corresponding LEED pattern is reported in Figure 3a, and shows six elongated spots forming an hexagonal cell corresponding to an incommensurate 2H-WS_2 film,

DOI: 10.1021/acs.chemmater.5b01170
Chem. Mater. 2015, 27, 4105−4113

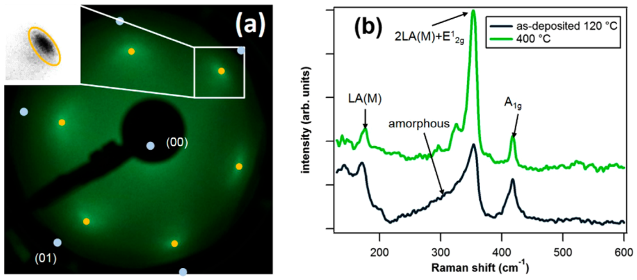

Figure 3. (a) LEED image acquired at 60 eV of WS_2/Au/Ni(111) deposited at 400 °C, inset showing a magnified view of a typical WS_2 diffraction spot; the white circles indicate calculated positions of Ni(111) diffraction spots. (b) Raman spectra of WS_2/Au/Ni(111) acquired with an excitation wavelength of 532 nm, before and after annealing at 400 °C.

whereas the substrate diffraction spots are heavily attenuated indicating that a fully covering monolayer film has formed.[43] The diffraction spots are about 10° wide, (see the inset in Figure 3a) indicating the presence of several rotational domains characterized by a small angle misalignment between the lattices of substrate and overlayer, similar to what was reported for the WS_2/HOPG system.[43] For low WS_2 coverage, several S/Au(111) reconstructions are detectable, as well.[49,50]

The presence of 2H-WS_2, after annealing at 400 °C, was confirmed by ex situ Raman spectra reported in Figure 3b. Three principal peaks are visible: the first one at 176 cm^{-1} corresponds to the longitudinal acoustic mode (LA(M)), the second one at 354 cm^{-1} originates from the overlap of the second order mode 2LA(M) and the $E_{2g}(\Gamma)$, whereas the third one at 417 cm^{-1} corresponds to the first order $A_{1g}(\Gamma)$. Moreover, the intensity ratio of the peaks at 354 and 417 cm^{-1} confirms the presence of predominantly single layer 2H-WS_2.[3] For the low temperature growth, the characteristic peaks of 2H-WS_2 are still well recognizable, but their fwhm is larger than that in the annealed sample, confirming a quite disordered structure. In the as-prepared samples, no features at lower wavenumbers corresponding to 1T-WS_2 have been detected.[10] Because of the clearly discernible Raman features of 2H-WS_2, we suggest the presence of a mixed phase where small seed crystals of 2H-WS_2 coexist with amorphous WS_2. As the sample is annealed, the amorphous areas can rearrange and grow off the already formed 2H seed crystals.

W 4*f* photoemission spectra can be separated into three single components, two related to WS_2, and the third to WS_3. The W $5p_{3/2}$ XPS line is found in the same spectral region of the W 4*f* photoemission line, which results in a broad component in the higher BE tail of the W 4*f* photoemission line (see brown component in Figure 2); the BEs for each component W $4f_{7/2}$ lines are reported in Table 1. Comparing the LEED and Raman data (Figure 3) and the XPS literature data, we assigned the lower BE WS_2 component to an amorphous phase and the higher BE one to the 2H-WS_2 phase. The W 4*f* photoemission line of a WS_2 layer deposited directly at 400 °C and separated into chemically shifted components, shows a predominant peak at 32.3 eV, which accounts for 88% of the whole photoemission spectrum. In Figure 4, the percentage of composition for each component of the W 4*f* photoemission line as a function of annealing temperature is reported (dots with the same color code reported in Figure 2).

Table 1. Binding Energies (eV) for the Different Components of the W $4f_{7/2}$ Photoemission Lines for WS_2/Au/Ni(111) and WS_2/h-BN/Au/Ni(111)

	amorphous WS_2[53]	2H-WS_2[10]	WS_3[54]
WS_2/Au/Ni(111)	31.6	32.3	33.6
WS_2/h-BN/Au/Ni(111)	31.7	32.4	33.6

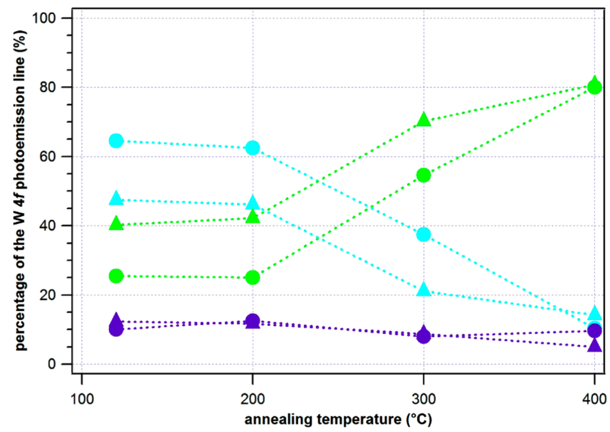

Figure 4. Percentage composition of amorphous WS_2, 2H-WS_2, and WS_3 on the W 4*f* photoemission lines for WS_2/Au/Ni(111) (circles) and WS_2/h-BN/Au/Ni(111) (triangles). The color code is the same as that in Figure 2.

As mentioned in the introduction, the layer deposited at low temperature exhibits W4*f* BEs comparable with the values expected for the 1T-WS_2 phase.[10,39,41] However, due to the lack of order seen by LEED and to the Raman data (see Figure 3), the XPS data are better interpreted as evidence of an amorphous WS_2 layer. It is clear from Figure 4 that thermal treatment transforms the amorphous WS_2 layer into the 2H-WS_2 phase. The presence of a component related to WS_3 in XPS data, which remains constant with annealing temperature (Figure 4), can be explained as nonstoichiometric, sulfur-rich WS_{2+x} species formed at the edges of WS_2 islands. In Raman spectra, amorphous WS_3 species, which are characterized by a spectral fingerprint at 460 and 520 cm^{-1},[51] were not detected suggesting that WS_3 is not a reaction intermediated of the formation of 2H-WS_2, as it is in the sulfurization of WO_3 to WS_2,[51] or the decomposition of $(NH_4)_2WS_4$.[52]

In the VB UPS data of the sample deposited at 120 °C (Figure 5), we can observe a strong attenuation of the substrate

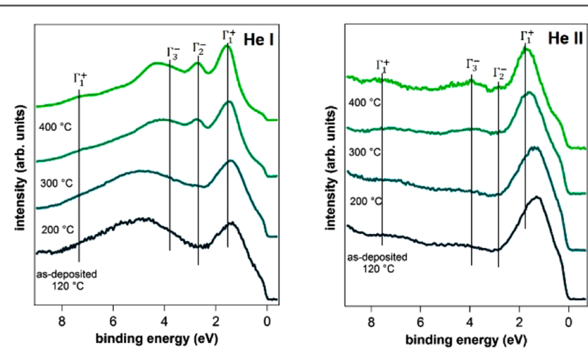

Figure 5. VB photoemission spectra of WS_2/Au/Ni(111) as-deposited at 120 °C and subsequently annealed at higher T in UHV, acquired with He I (21.2 eV, pass energy = 2 eV) and He II (40.8 eV, pass energy = 10 eV). The features were linked to symmetry of S *p* orbitals based on ref 43.

DOI: 10.1021/acs.chemmater.5b01170
Chem. Mater. 2015, 27, 4105−4113

bands due to the presence of a fully covering WS2 single layer film and the appearance of new broad features at about 1.3, 4.4, and 6.9 eV. After annealing at 300−400 °C, these peaks become sharper and slightly shift their BE positions to 1.7, 3.9, and 7.4 eV, respectively, while a new state appears at 2.8 eV. All of these features can be labeled according to the symmetry driven combinations between W 5*d* and S 3*p* orbitals (space group $P\bar{6}m2(D^1_{3h})$ (see Figure 6). The latter in monolayer 2H-WS_2 can combine into four bands with different symmetries, i.e., Γ_1^+, Γ_2^-, Γ_3^-. In 2H-WS_2 and more generally in most TMDs, there is a pronounced hybridization between the chalcogenide *p* and the metal *d* orbitals.[55,56] The electronic states that characterize the VB maximum, stem from the hybridization between p_z (Γ_1^+ and Γ_2^-) and d_{z^2} states.[57] Moreover, the d_{xy} and $d_{x^2-y^2}$ metal orbitals mix with the Γ_3^+ state, whereas the d_{xz} and d_{yz} interact with the Γ_3^-.[43] As in a previous work,[43] the transition involving Γ_3^+ is difficult to discern because of the low photoionization cross section.

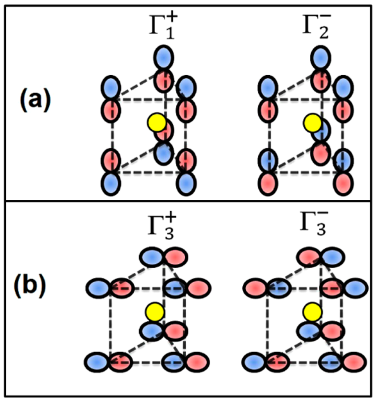

Figure 6. Symmetry combinations of (a) p_z and (b) p_x/p_y sulfur orbitals in a monolayer 2H-WS_2 unit cell with symmetry labels used for the irreducible representations of the space group $P\bar{6}m2(D^1_{3h})$.

Growth of WS_2/h-BN/Au/Ni(111). In order to grow single layer WS_2 on a quasi-freestanding, ultrathin insulator, WS_2 was grown on h-BN decoupled from Ni(111) by few Au layers (WS_2/h-BN/Au/Ni(111)).

WS_2 was grown at 120 °C and then annealed at 200 °C, 300 °C, and 400 °C. The growth of coherent and ordered interfaces in the WS_2/h-BN/Au/Ni(111) system is difficult because the h-BN layer must be of high quality in order to serve as a good epitaxial substrate for the growth of an ordered WS_2 layer, as reported for WS_2/HOPG.[43] In the best conditions, as shown in Figure 7a, the experimental LEED pattern of this heterostructure presents six incommensurate, but azimuthally oriented spots with the spacing expected for 2H-WS_2,[33] which is qualitatively similar to the WS_2/Au/Ni(111) system reported in Figure 3a, this LEED pattern demonstrates the presence of van der Waals epitaxy. Unfortunately, the low image quality makes any precise unit cell estimation unreliable, thus preventing the determination of possible strain or layer relaxation. Also in this case, no LEED pattern was observed for WS_2 grown at 120 °C, further confirming the presence of a prevalent amorphous structure.

Comparing the Raman spectra of WS_2/Au/Ni(111) and WS_2/h-BN/Au/Ni(111), Figures 3 and 7, the features for the as-prepared sample indicate a more disordered layer in the case of WS_2/h-BN/Au/Ni(111). After annealing, the peaks have a higher fwhm with respect to those of the WS_2/Au/Ni(111) system. As in the case of WS_2/Au, because of the presence of 2H features in Raman spectra, it is likely that 2H-WS_2 nanodomains form at low temperature and serve as a seeds during annealing. Therefore, combined evidence from LEED and Raman spectroscopy (Figure 3 vs Figure 7) shows that Au has a higher templating effect than h-BN for the growth of 2H-WS_2. This can be explained by assuming that the interaction between the WS_2 and h-BN is very weak, whereas the interaction with Au is stronger. This is in agreement with previous experiments on the growth of MoS_2 on Au(111) and HOPG, while in the case of Au(111) the interaction with the substrate is stronger and a clear epitaxial relationship is observed, in the case of HOPG disorder is enhanced.[58,59]

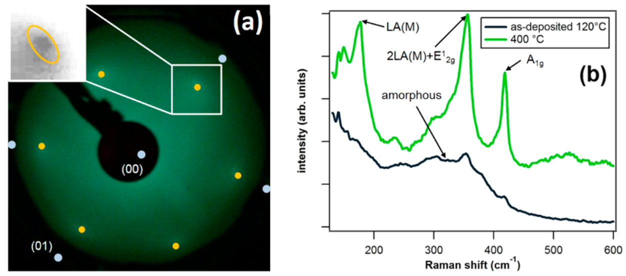

Figure 7. (a) LEED image acquired at 60 eV of WS_2/h-BN/Au/Ni(111) after annealing, the inset reports a magnified view of a WS_2 diffraction spot, white circles indicate calculated positions of Ni(111) diffraction spots. (b) Raman spectra of WS_2/h-BN/Au/Ni(111) acquired with an excitation wavelength of 532 nm, before and after annealing at 400 °C.

Also in this case, the disappearance of the diffraction spots of the substrate in the LEED pattern and the intensity ratio between the bands at 354 and 417 cm^{-1} less than one[3] indicate the presence of single layer WS_2.

XPS data indicate a similar trend in phase structure for WS_2/h-BN/Au/Ni(111) compared to WS_2/Au/Ni(111) the fraction of the 2H-phase increases with increasing annealing temperature (Figure 4). Interestingly, for the WS_2/h-BN/Au/Ni(111) system, the WS_3 photoemission signals decrease with annealing temperature. Indeed, dosing in our conditions (2×10^{-8} mbar at 400 °C for 15 min.) on Au (∼6 ML)/Ni(111) results in various stable superstructures.[49,50] We speculate that WS_3 is abundant at the edges of the WS_2 nanoparticles. Therefore, because of the lower affinity for S to bind to h-BN, the formation of a nonstoichiometric, sulfur-rich WS_{2+x} is unfavorable with respect to Au.

Interestingly, the W 4*f* photoemission spectra corresponding to amorphous and 2H-WS_2 are shifted 0.1 eV to higher BEs with respect to the WS_2/Au/Ni(111), while maintaining their separation of 0.7 eV, indicating a slightly different electronic coupling, see Table 1. Additionally, the VB UPS data of the monolayer WS_2/h-BN/Au/Ni(111) (Figure 9), show features very similar to those reported for WS_2/Au/Ni(111) (Figure 5). The spectra are mostly dominated by the presence of the outermost layer of WS_2 as expected for a fully covering single layer films; however, they show a barely visible additional state at ∼4.35 eV related to the σ band of quasi-freestanding h-BN (see Figure 1c).[44,48] Even when WS_2 is placed on an insulator, there is no large energy shift of its bands with respect to WS_2/Au. This can be explained by the absence of strong interlayer coupling between WS_2 and both Au and h-BN.[23−25] Similar to WS_2/Au/Ni(111), annealing at high temperature leads to a transition from broad spectral features to sharper ones, which is

DOI: 10.1021/acs.chemmater.5b01170
Chem. Mater. 2015, 27, 4105−4113

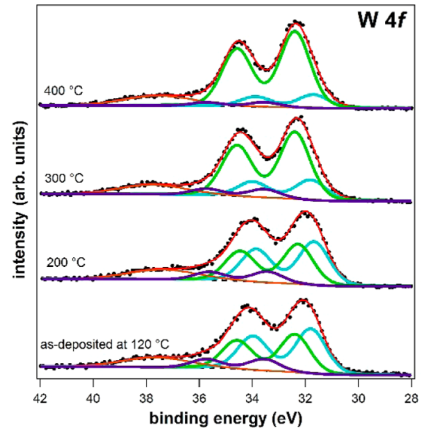

Figure 8. W 4*f* photoemission spectra of WS_2/h-BN/Au/Ni(111) as-deposited at 120 °C and subsequently annealed at 200 °C, 300 °C, and 400 °C. Measured data, Shirley background and total fit are represented with black dots, dashed black line, and solid red line, respectively. Photoemission lines of amorphous WS_2, 2H-WS_2, WS_3, W $5p_{3/2}$ are shown with blue, green, purple, and brown solid lines, respectively.

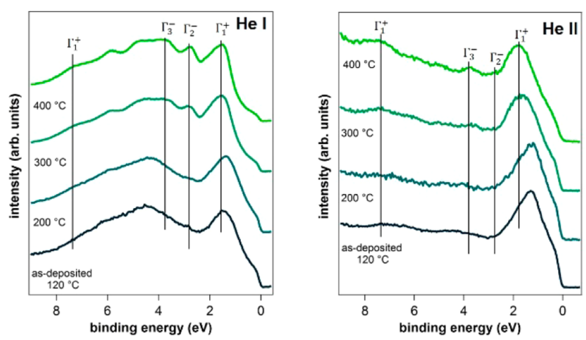

Figure 9. VB spectra of WS_2/h-BN/Au/Ni(111) as-deposited at 120 °C and subsequently annealed at higher T in UHV, acquired with He I (21.2 eV, pass energy = 2 eV) and He II (40.8 eV, pass energy = 10 eV). The features were linked to symmetry of S *p* orbitals based on ref 43.

correlated with Raman spectroscopy (Figure 7), indicating a transition from predominantly amorphous to single layer 2H-WS_2. For the as-deposited layer, Raman spectra show a broad band centered at ~300 cm^{-1}, but there are still small peaks present in the position of 2H-WS_2. For the as-deposited sample of WS_2/Au/Ni(111), there are no clear Raman features of 1T-WS_2 or of WS_3 which suggests a growth mechanism similar to that on the Au/Ni(111) substrate.

Recently, ARPES revealed the opening of a mini-gap in the graphene π orbitals with the out-of-plane states of the TMDC when placed on an MoS_2 single crystal.[60] We investigated by ARPES with variable-polarization synchrotron radiation an in situ grown WS_2/h-BN heterostructure, in order to identify the band character of our stacked materials and the presence of possible modifications induced by interfacial interactions. The VB spectra of 1 ML of WS_2 deposited on h-BN/Au/Ni(111) along the Γ−M direction with two perpendicular linear polarizations are reported in Figure 10a,b. Since the angle of light incidence on the sample surface is 45°, a linear horizontal polarization vector can be decomposed in two components in and out of the surface plane, while the linear vertical polarization is mainly in the surface plane and along the dispersion direction. We identify three main band structure

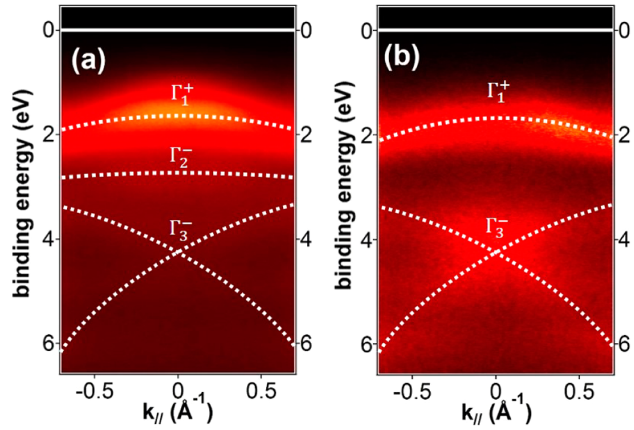

Figure 10. ARPES spectra obtained with synchrotron light at 40 eV with (a) linear horizontal polarization and (b) linear vertical polarization. The features were linked to the symmetry of S 3*p* orbitals based on ref 43.

features at 1.5, 2.8, and 4 eV at the Γ point. Notably, the absence of a band (Γ_4^-) at ~1 eV is a distinctive electronic feature of single layer WS_2.[43]

The first band at 1.5 eV originates from the hybridization of W $5d_{z^2}$ and Γ_1^+ S $3p_z$ orbitals, (see Figure 6) and is particularly emphasized with horizontal polarization (out of surface plane). The second band, at 2.8 eV, can be observed with horizontally polarized radiation and comes from symmetrically different p_z, orbitals (Γ_2^-). The third feature visible in Figure 10a, derives from the Γ_3^- states mixed with W d_{xz} and d_{yz} orbitals. These states generate two distinct bands that cross in the Γ point at a BE of 4 eV. The use of linearly polarized radiation in the surface plane suppresses the band at 1.5 eV, whereas the band at 2.8 eV becomes almost undetectable. On the contrary, the bands that are a result of the hybridization of p_x and p_y orbitals, Γ_3^-, become highly emphasized.[43]

It is interesting to observe that the energy separation between the bands at the Γ point is the same as that observed for UHV exfoliated WS_2 single crystal or epitaxial WS_2 films grown in situ on HOPG under UHV conditions.[43] This indicates the extremely good quality of our films: operating in UHV conditions allows the elimination of any source of contamination and the preparation of films with low defect concentration, which therefore are very prone to any electronic interaction. Monolayer WS_2 supported on h-BN (insulator), HOPG (semimetal), or Au (metal) presents very similar electronic structure. For this reason, an efficient modulation of the electronic properties requires alternative approaches to van der Waals epitaxy.

CONCLUSIONS

We studied the growth of a WS_2 monolayer on gold and on quasi-freestanding h-BN by using XPS, UPS, Raman spectroscopy, and LEED. The latter indicates that although the WS_2 film is incommensurate with respect to the substrate, there is evidence for van der Waals epitaxy. Nevertheless, photoemission VB measurements reveal the absence of interlayer coupling, so that WS_2 supported either on insulating h-BN or metal Au presents the same electronic structure. This outcome is not unexpected considering the high chemical perfection and absence of any possible contaminants in systems grown under UHV conditions. These results suggest that Au is a perfect candidate for the preparation of metal contacts, whereas h-BN

DOI: 10.1021/acs.chemmater.5b01170
Chem. Mater. 2015, 27, 4105−4113

can be used as an ideal substrate to support monolayer WS_2 with the aim of keeping intact its intrinsic properties such as photoluminescence.[61]

The WS_2 film deposited at low temperature on both substrates shows a W 4*f* photoemission line centered at BE very close to the values reported in the literature for 1T-WS_2.[10,39,41] However, our data indicate that similar spectra can be obtained on amorphous WS_2 that can be converted to crystalline 2H-WS_2 after annealing at 300−400 °C. For the as-deposited samples (at 120 °C), our data suggest the formation of a mixed phase, i.e., primarily an amorphous phase with crystalline 2H-WS_2 seeds. Therefore, our data suggest that amorphous WS_2 could be erroneously identified as 1T-WS_2 on the basis of the simple XPS fingerprint. This must be taken into account when XPS measurements are used as a quantitative technique to estimate the 1*T*/2H ratio in WS_2-based materials.

Finally, our method for growing heterostructures under UHV conditions can be exploited as a quite general strategy to synthesize and study the pristine properties of other artificially stacked materials. For example, graphene can be grown on Ni(111) and decoupled with gold,[62] as done here for h-BN; tungsten can be replaced by other transition metals, i.e., Mo or Ni, so that a full gamut of TMDs can be easily obtained. This provides an alternative and more reliable route with respect to ex situ CVD synthesis or mechanical transfer method, for the fundamental study of the authentic properties of complex heterostructures.

■ AUTHOR INFORMATION

Corresponding Author

* Tel.: +39 049 8275122. E-mail: stefano.agnoli@unipd.it.

Notes

The authors declare no competing financial interest.

■ ACKNOWLEDGMENTS

This work was partially supported by the Italian MIUR through the national grant Futuro in Ricerca 2012 RBFR128BEC "Beyond graphene: tailored C-layers for novel catalytic materials and green chemistry" and by the University of Padova funded project: CPDA128318/12 "Study of the catalytic activity of complex graphene nanoarchitectures from ideal to real conditions" and through the grant "Attrezzature scientifiche finalizzate alla ricerca—Bando 2012". B.M. acknowledges the Pennsylvania State University International Internship in Materials program that enabled this work at the University of Padova.

■ REFERENCES

(1) Novoselov, K. S.; Geim, A. K.; Morozov, S. V.; Jiang, D.; Zhang, Y.; Dubonos, S. V.; Grigorieva, I. V.; Firsov, A. A. Electric field effect in atomically thin carbon films. *Science* **2014**, *306*, 666.

(2) Chhowalla, M.; Suk Shin, H.; Eda, G.; Li, L. J.; Loh, K. P.; Zhang, H. The chemistry of two-dimensional layered transition metal dichalcogenide sheets. *Nat. Chem.* **2013**, *5*, 263.

(3) Berkdemir, A.; Gutiérrez, H. R.; Botello-Méndez, A. R.; Perea-López, N.; Elías, A. L.; Chia, C. I.; Wang, B.; Crespi, V. H.; López-Urías, F.; Charlier, J. C.; Terrones, H.; Terrones, M. Identification of few layers of WS_2 using Raman spectroscopy. *Sci. Rep.* **2013**, *3*, 1755.

(4) Mak, K. F.; Lee, C.; Hone, J.; Shan, J.; Heinz, T. F. Atomically thin MoS_2: A new direct-gap semiconductor. *Phys. Rev. Lett.* **2010**, *105*, 136905.

(5) Geim, A. K.; Grigorieva, I. V. Van der Waals heterostructures. *Nature* **2013**, *499*, 419.

(6) Xu, X.; Yao, W.; Xiao, D.; Heinz, T. F. Spin and pseudospins in layered transition metal dichalcogenides. *Nat. Phys.* **2014**, *10*, 343.

(7) Janisch, C.; Wang, Y.; Ma, D.; Mehta, N.; Elías, A. L.; Perea-López, N.; Terrones, M.; Crespi, V.; Liu, Z. Extraordinary Second Harmonic Generation in tungsten disulfide monolayers. *Sci. Rep.* **2014**, *4*, 5530.

(8) Riley, J. M.; Mazzola, F.; Dendzik, M.; Michiardi, M.; Takayama, T.; Bawden, F.; Granerød, C.; Leandersson, M.; Balasubramanian, T.; Hoesch, M.; Kim, T. K.; Takagi, H.; Meevasana, W.; Hofmann, Ph.; Bahramy, M. S.; Wells, J. W.; King, P. D. C. Direct observation of spin-polarized bulk bands in an inversion-symmetric semiconductor. *Nat. Phys.* **2014**, *10*, 835.

(9) Thakur, D. S.; Delmon, B. The role of group VIII metal promoter in MoS_2 and WS_2 hydrotreating catalysts: I. ESR studies of CoMo, NiMo, and NiW catalysts. *J. Catal.* **1985**, *91*, 308.

(10) Voiry, D.; Yamaguchi, H.; Li, J.; Silvia, R.; Alves, D. C. B.; Fujita, T.; Chen, M.; Asefa, T.; Shenoy, V.; Eda, G.; Chowalla, M. Enhanced Catalytic Activity in Strained Chemically Exfoliated WS2 Nanosheets for Hydrogen Evolution. *Nat. Mater.* **2013**, *12*, 850.

(11) Jaramillo, T. F.; Jørgensen, K. P.; Bonde, J.; Nielsen, J. H.; Horch, S. Identification of active edge sites for electrochemical H2 evolution from MoS_2 nanocatalysts. *Science* **2007**, *317*, 100.

(12) Kubota, Y.; Watanabe, K.; Tsuda, O.; Taniguchi, T. Deep Ultraviolet Light-Emitting Hexagonal Boron Nitride Synthesized at Atmospheric Pressure. *Science* **2007**, *317*, 932.

(13) Kim, K. K.; Hsu, A.; Jia, X.; Kim, S. M.; Shi, Y.; Hofmann, M.; Nezich, D.; Rodriguez-Nieva, J. F.; Dresselhaus, M.; Palacios, T.; Kong, J. Synthesis of monolayer hexagonal boron nitride on Cu foil using chemical vapor deposition. *Nano Lett.* **2012**, *12*, 161.

(14) Yingjie Tay, R.; Griep, M. H.; Mallick, G.; Tsang, S. H.; Singh, R. S.; Tumlin, T.; Tong Teo, E. H.; Karna, S. P. Growth of large single-crystalline two-dimensional boron nitride hexagons on electropolished copper. *Nano Lett.* **2014**, *14*, 839.

(15) Shi, Y.; Hamsen, C.; Jia, X.; Kang Kim, K.; Reina, A.; Hofmann, M.; Long Hsu, A.; Zhang, K.; Li, H.; Juang, Z. Y.; Dresselhaus, M. S.; Li, L. J.; Kong, J. Synthesis of few layer hexagonal boron nitride thin film by chemical vapor deposition. *Nano Lett.* **2010**, *10*, 4134.

(16) Bresnehan, M. S.; Hollander, M. J.; Wetherington, M.; Wang, K.; Miyagi, T.; Pastir, G.; Snyder, D. W.; Gengler, J. J.; Voevodin, A. A.; Mitchel, W. C.; Robinson, J. A. Prospects of direct growth boron nitride films as substrates for graphene electronics. *J. Mater. Res.* **2014**, *29*, 459.

(17) Joshi, N.; Ghosh, P. Substrate-induced changes in the magnetic and electronic properties of hexagonal boron nitride. *Phys. Rev. B* **2013**, *87*, 235440.

(18) Britnell, L.; Gorbachev, R. V.; Jalil, R.; Belle, B. D.; Schedin, F.; Mishchenko, A.; Georgiou, T.; Katsnelson, M. I.; Eaves, L.; Morozov, S. V.; Peres, N. M. R.; Leist, J.; Geim, A. K.; Novoselov, K. S.; Ponomarenko, L. A. Field-effect tunneling transistor based on vertical graphene heterostructures. *Science* **2012**, *335*, 947.

(19) Gannett, W.; Regan, W.; Watanabe, K.; Taniguchi, T.; Crommie, M. F.; Zettl, A. Boron nitride substrates for high mobility chemical vapor deposited graphene. *Appl. Phys. Lett.* **2011**, *98*, 242105.

(20) Georgiou, T.; Jalil, R.; Belle, B. D.; Britnell, L.; Gorbachev, R. V.; Morozov, S. V.; Kim, Y.-J.; Gholinia, A.; Haigh, S. J.; Makarovsky, O.; Eaves, L.; Ponomarenko, L. A.; Geim, A. K.; Novoselov, K. S.; Mishchenko, A. Vertical field-effect transistor based on graphene-WS2 heterostructures for flexible and transparent electronics. *Nat. Nanotechnol.* **2013**, *8*, 100.

(21) Yu, W. J.; Liu, Y.; Zhou, H.; Yin, A.; Li, Z.; Huang, Y.; Duan, X. Highly efficient gate-tunable photocurrent generation in vertical heterostructures of layered materials. *Nat. Nanotechnol.* **2013**, *8*, 952.

(22) Lee, C.; Hong, J.; Whangbo, M.-H.; Shim, J. H. Enhancing the Thermoelectric Properties of Layered Transition-Metal Dichalcogenides 2H-MQ_2 (M = Mo, W; Q = S, Se, Te) by Layer Mixing: Density Functional Investigation. *Chem. Mater.* **2013**, *25*, 3745.

(23) Tongay, S.; Fan, W.; Kang, J.; Park, J.; Koldemir, U.; Suh, J.; Narang, D. S.; Liu, K.; Ji, J.; Li, J.; Sinclair, R.; Wu, J. Tuning Interlayer

DOI: 10.1021/acs.chemmater.5b01170
Chem. Mater. 2015, 27, 4105−4113

Coupling in Large-Area Heterostructures with CVD Grown MoS_2 and WS_2 Monolayers. *Nano Lett.* **2014**, *14*, 3185.
(24) Yuan, J.; Najmaei, S.; Zhang, Z.; Zhang, J.; Lei, S.; Ajayan, P. M.; Yakobson, B. I.; Lou, J. Photoluminescence Quenching and Charge Transfer in Artificial Heterostacks of Monolayer Transition Metal Dichalcogenides and Few-Layer Black Phosphorus. *ACS Nano* **2015**, *9*, 555.
(25) Fang, H.; Battaglia, C.; Carraro, C.; Nemsak, S.; Ozdol, B.; Kang, J. S.; Bechtel, H. A.; Desai, S. B.; Kronast, F.; Unal, A. A. M.; Conti, G.; Conlon, C.; Palsson, G. K.; Martin, M. C.; Minor, A. M.; Fadley, C. S.; Yablonovitch, E.; Maboudian, R.; Javey, A. Strong interlayer coupling in van der Waals heterostructures built from single-layer chalcogenides. *Proc. Natl. Acad. Sci. U. S. A.* **2014**, *111*, 6198.
(26) Haigh, S. J.; Gholinia, A.; Jalil, R.; Romani, S.; Britnell, L.; Elias, D. C.; Novoselov, K. S.; Ponomarenko, L. A.; Geim, A. K.; Gorbachev, R. Cross-sectional imaging of individual layers and buried interfaces of graphene-based heterostructures and superlattices. *Nat. Mater.* **2012**, *11*, 764.
(27) Ambrosi, A.; Pumera, M. The CVD graphene transfer procedure introduces metallic impurities which alter the graphene electrochemical properties. *Nanoscale* **2014**, *6*, 472.
(28) Lin, Y.-C.; Lu, C.-C. L.; Yeh, C.-H.; Jin, C.; Suenaga, K.; Chiu, P.-W. Atomic mechanism of the semiconducting-to metallic phase transition in single-layered MoS_2. *Nano Lett.* **2012**, *12*, 414.
(29) Lin, Y.-C.; Lu, N.; Perea-Lopez, N.; Li, J.; Lin, Z.; Peng, X.; Lee, C. H.; Sun, C.; Calderin, L.; Browning, P. N.; Bresnehan, M. S.; Kim, M. J.; Mayer, T. S.; Terrones, M.; Robinson, J. A. Direct Synthesis of van der Waals Solids. *ACS Nano* **2014**, *8*, 3715.
(30) Lin, Y.-C.; Chang, C.-Y. S.; Ghosh, R. K.; Li, J.; Zhu, H.; Addou, R.; Diaconescu, B.; Ohta, T.; Peng, X.; Lu, N.; Kim, M. J.; Robinson, J. T.; Wallace, R. M.; Mayer, T. S.; Datta, S.; Li, L.-J.; Robinson, J. A.; Robinson, J. A. Atomically Thin Heterostructures Based on Single-Layer Tungsten Diselenide and Graphene. *Nano Lett.* **2014**, *14*, 6936.
(31) Eichfeld, S. M.; Hossain, L.; Lin, Y.-C.; Piasecki, A. F.; Kupp, B.; Birdwell, A. G.; Burke, R. A.; Lu, N.; Peng, X.; Li, J.; Azcatl, A.; McDonnell, S.; Wallace, R. M.; Kim, M. J.; Mayer, T. S.; Redwing, J. M.; Robinson, J. A. Highly Scalable, Atomically Thin WSe_2 Grown via Metal−Organic Chemical Vapor Deposition. *ACS Nano* **2015**, *9*, 2080.
(32) Shi, Y.; Zhou, W.; Lu, A.-Y.; Fang, W.; Lee, Y.-H.; Hsu, A. L.; Kim, S. M.; Kim, K. K.; Yang, H. Y.; Li, L.-J.; Idrobo, J.-C.; Kong, J. van der Waals Epitaxy of MoS_2 Layers Using Graphene As Growth Templates. *Nano Lett.* **2012**, *12*, 2784.
(33) Okada, M.; Sawazaki, T.; Watanabe, K.; Taniguch, T.; Hibino, H.; Shinohara, H.; Kitaura, R. Direct Chemical Vapor Deposition Growth of WS_2 Atomic Layers on Hexagonal Boron Nitride. *ACS Nano* **2014**, *8*, 8273.
(34) Gong, Y.; Lin, J.; Wang, X.; Shi, G.; Lei, S.; Lin, Z.; Zou, X.; Ye, G.; Vajtai, R.; Yakobson, B. I.; Terrones, H.; Terrones, M.; Tay, B. K.; Lou, J.; Pantelides, S. T.; Liu, Z.; Zhou, W.; Ajayan, P. M. Vertical and in-plane heterostructures from WS_2/MoS_2 monolayers. *Nat. Mater.* **2014**, *13*, 1135.
(35) Yue, R.; Barton, A. T.; Zhu, H.; Azcatl, A.; Pena, L. F.; Wang, J.; Peng, X.; Lu, N.; Cheng, L.; Addou, R.; McDonnell, S.; Colombo, L.; Hsu, J. W. P.; Kim, J.; Kim, M. J.; Wallace, R. M.; Hinkle, C. L. $HfSe_2$ Thin Films: 2D Transition Metal Dichalcogenides Grown by Molecular Beam Epitaxy. *ACS Nano* **2015**, *9*, 474.
(36) Ganatra, R.; Zhang, Q. Few-Layer MoS_2: A Promising Layered Semiconductor. *ACS Nano* **2014**, *8*, 4074.
(37) Lin, Y.-C.; Dumcenco, D. O.; Huang, Y.-S.; Suenaga, K. Atomic mechanism of the semiconducting-to metallic phase transition in single-layered MoS_2. *Nat. Nanotechnol.* **2014**, *9*, 391.
(38) Wang, H.; Zhang, Q.; Yao, H.; Liang, Z.; Lee, H. W.; Hsu, P. C.; Zheng, G.; Cui, Y. High electrochemical selectivity of edge versus terrace sites in two-dimensional layered MoS_2 materials. *Nano Lett.* **2014**, *14*, 7138.
(39) Mahler, B.; Hoepfner, V.; Liao, K.; Geoffrey, A. O. Colloidal Synthesis of 1T-WS_2 and 2H-WS_2 Nanosheets: Applications for Photocatalytic Hydrogen Evolution. *J. Am. Chem. Soc.* **2014**, *136*, 14121.
(40) Enyashin, A. N.; Yadgarov, L.; Houben, L.; Popov, I.; Weidenbach, M.; Tenne, R.; Bar-Sadan, M.; Seifert, G. New Route for Stabilization of 1T-WS_2 and MoS_2 Phases. *J. Phys. Chem. C* **2011**, *115*, 24586.
(41) Eng, A. Y. S.; Ambrosi, A.; Sofer, Z.; Simek, P.; Pumera, M. Electrochemistry of Transition Metal Dichalcogenides: Strong Dependence on the Metal-to-Chalcogen Composition and Exfoliation Method. *ACS Nano* **2014**, *8*, 12185.
(42) Fuchtbauer, H. G.; Tuxen, A. K.; Moses, P. G.; Topsøe, H.; Besenbacher, F.; Lauritsen, J. V. Morphology and atomic-scale structure of single-layer WS_2 nanoclusters. *Phys. Chem. Chem. Phys.* **2013**, *15*, 15971.
(43) Klein, A.; Tiefenbacher, S.; Eyert, V.; Pettenkofer, C.; Jaegermann, W. Electronic band structure of single-crystal and single-layer WS2: Influence of interlayer van der Waals interactions. *Phys. Rev. B* **2001**, *64*, 205416.
(44) Usachov, D.; Adamchuk, V. K.; Haberer, D.; Grüneis, A.; Sachdev, H.; Preobrajenski, A. B.; Laubschat, C.; Vyalikh, D. V. Quasifreestanding single-layer hexagonal boron nitride as a substrate for graphene synthesis. *Phys. Rev. B* **2010**, *82*, 075415.
(45) Berkowitz, J.; Marquardt, J. R. Equilibrium Composition of Sulphur Vapor. *J. Chem. Phys.* **1963**, *39*, 275.
(46) Fadley, C. S. Angle-resolved X-ray photoelectron spectroscopy. *Prog. Surf. Sci.* **1984**, *16*, 275.
(47) Jash, P.; Meaux, K.; Trenary, M. Transmission Infrared Spectroscopy of Ammonia Borane. *J. Undergrad. Res.* **2012**, *5*, 1.
(48) Nagashima, A.; Tejima, N.; Gamou, Y.; Kawai, T.; Oshima, C. Electronics states of monolayer hexagonal boron nitride formed on the metal surfaces. *Surf. Sci.* **1996**, *357*−*358*, 307.
(49) McGuirk, G. M.; Shin, H.; Caragiu, M.; Ash, S.; Bandyopadhyay, P. K.; Prince, R. H.; Diehl, R. D. Au(111) surface structures induced by adsorption: LEED I(E) analysis of (1×1) and (5×5) Au(111)-S phases. *Surf. Sci.* **2013**, *610*, 42.
(50) Lay, M. D.; Varazo, K.; Stickney, J. L. Formation of sulfur atomic layers on gold from aqueous solutions of sulfide and thiosulfate: Studies using EC-STM, UHV-EC, and TLEC. *Langmuir* **2003**, *19*, 8416.
(51) Payen, E.; Kasztelan, S.; Grimblot, J.; Bonnelle, J. P. Study of the sulphurization of WO_3/ γ-Al_2O_3 catalysts by in situ laser raman spectroscopy. *Catal. Today* **1988**, *4*, 57.
(52) Walton, R. I.; Hibble, S. J. A combined in situ X-ray absorption spectroscopy and X-ray diffraction study of the thermal decomposition of ammonium tetrathiotungstate. *J. Mater. Chem.* **1999**, *9*, 1347.
(53) Zabinski, J. S.; Donley, M. S.; Prasad, S. V. Synthesis and characterization of tungsten disulphide films grown by pulsed-laser deposition. *J. Mater. Sci.* **1994**, *29*, 4834.
(54) Khudorozhko, G. F.; Asanov, I. P.; Mazalov, L. N.; Kravtsova, E. A.; Parygina, G. K.; Fedorov, V. E.; Mironov, J. V. The study of electronic structure of molybdenum and tungsten trisulfides and their lithium intercalates by X-ray electron and X-ray emission and absorption spectroscopy. *J. Electron Spectrosc. Relat. Phenom.* **1994**, *68*, 199.
(55) Bromley, R. A.; Murray, R. B.; Yoffe, A. D. The band structures of some transition metal dichalcogenides. III. Group VIA: trigonal prism materials. *J. Phys. C: Solid State Phys.* **1972**, *5*, 759.
(56) Mattheiss, L. F. Band Structures of Transition-Metal-Dichalcogenide Layer Compounds. *Phys. Rev. B* **1973**, *8*, 3719.
(57) Coehoorn, R.; Haas, C.; Dijkstra, J.; Flipse, C. J. F.; de Groot, R. A.; Wold, A. Electronic structure of $MoSe_2$, MoS_2, and WSe_2. I. Band-structure calculations and photoelectron spectroscopy. *Phys. Rev. B* **1987**, *35*, 6195.
(58) Kibsgaard, J.; Lauritsen, J. V.; Clausen, B. S.; Topsøe, H.; Besenbacher, F. Cluster-support interactions and morphology of MoS_2 nanoclusters in a graphite-supported hydrotreating model catalyst. *J. Am. Chem. Soc.* **2006**, *128*, 13950.
(59) Walton, A. S.; Lauritsen, J. V.; Topsøe, H.; Besenbacher, F. MoS_2 nanoparticle morphologies in hydrodesulfurization catalysis studied by scanning tunneling microscopy. *J. Catal.* **2013**, *308*, 306.

DOI: 10.1021/acs.chemmater.5b01170
Chem. Mater. 2015, 27, 4105−4113

(60) Coy Diaz, H.; Avila, J.; Chen, C.; Addou, R.; Asensio, M. C.; Batzill, M. Artificially Stacked Atomic Layers: Toward New van der Waals Solids. *Nano Lett.* **2015**, *15*, 1135.
(61) Gutiérrez, H. R.; Perea-López, N.; Elías, A. L.; Berkdemir, A.; Wang, B.; Lv, R.; López-Urías, F.; Crespi, V. H.; Terrones, H.; Terrones, M. Extraordinary Room-Temperature Photoluminescence in Triangular WS_2 Monolayers. *Nano Lett.* **2012**, *13*, 3447.
(62) Varykhalov, A.; Sánchez-Barriga, J.; Shikin, A. M.; Biswas, C.; Vescovo, E.; Rybkin, A.; Marchenko, D.; Rader, O. Electronic and Magnetic Properties of Quasifreestanding Graphene on Ni. *Phys. Rev. Lett.* **2008**, *101*, 157601.

DOI: 10.1021/acs.chemmater.5b01170
Chem. Mater. 2015, 27, 4105−4113